Available online at www.sciencedirect.com

SciVerse ScienceDirect

journal homepage: www.elsevier.com/locate/he

Preparation and characterization of imidazolium-functionalized poly (ether sulfone) as anion exchange membrane and ionomer for fuel cell application

Wangting Lu [a,b], Zhi-Gang Shao [a,*], Geng Zhang [a,b], Yun Zhao [a,b], Jin Li [a,b], Baolian Yi [a]

[a] Fuel Cell System and Engineering Group, Dalian Institute of Chemical Physics, Chinese Academy of Sciences, 457 Zhongshan Road, 116023 Dalian, PR China

[b] Graduate School of Chinese Academy of Sciences, 19A Yuquan Road, 100049 Beijing, PR China

ARTICLE INFO

Article history:
Received 22 December 2012
Received in revised form
9 May 2013
Accepted 9 May 2013
Available online 14 June 2013

Keywords:
Anion exchange membrane
Anion exchange ionomer
Fuel cell
Imidazolium
Poly (ether sulfone)

ABSTRACT

Imidazolium-functionalized anion exchange membranes (AEMs) for anion exchange membrane fuel cells (AEMFCs) were synthesized by functionalization of chloromethylated poly (ether sulfone) (PES) with 1-alkylimidazole. The properties of AEMs can be controlled by the degree of chloromethylation of PES. Moreover, with the increment of the alkyl line length on the imidazolium group, the water uptake, swelling ratio and solubility of AEMs increased, whereas the hydroxide conductivity declined. By dissolving AEMs in the mixture of ethanol and water, IM-based anion exchange ionomers (AEIs) can be obtained. Electrochemical studies revealed that the catalytic activities of Pt/C towards oxygen reduction and hydrogen oxidation in the presence of imidazolium-functionalized AEIs were almost the same with that of commercial quaternary ammonium-based ionomers. The fabricated AEM and AEI were utilized to assemble H_2/O_2 AEMFC, yielding a peak power density of ~30 mW cm^{-2} with open circuit potential larger than 1.0 V. The results obtained indicate that imidazolium-functionalized AEMs and AEIs may be candidates which are worth further investigation for the application in the AEMFCs.

1. Introduction

In the near past decades, considerable attention has been paid to fuel cells because of high efficiency and low pollution levels. As especially developed for portable and electric vehicle applications, proton exchange membrane fuel cells (PEMFCs) received much attention and preferential development [1]. However, the utilization of Pt based cathode electrocatalysts has become one of the obstacles that impede the large-scale commercialization of PEMFCs [2]. Compared with PEMFCs, numerous advantages, such as faster oxygen reduction reaction (ORR) kinetics, desirable applicability of non-precious metals as catalyst and milder corrosion environment [3,4], can be achieved under alkaline conditions. Therefore, increasing interests were attached to the exploitation of AEMFCs. Therein, AEM and AEI play inherently

* Corresponding author. Tel.: +86 411 84379153; fax: +86 411 84379185.
E-mail address: zhgshao@dicp.ac.cn (Z.-G. Shao).

0360-3199/$ – see front matter
http://dx.doi.org/10.1016/j.ijhydene.2013.05.070

significant roles in improving fuel cell performance. The AEM transports hydroxide from the cathode to the anode and prevents the mix of reactants. The AEI was used to provide hydroxide conducting channels in the electrode to build three-phase boundaries where electrochemical reaction takes place [5].

Up to now, the quaternary ammonium (QA) has been the most extensively studied anion conductive head groups in AEMs [3,6]. However, the QA groups are usually suffered from poor solubility in low-boiling-point solvents [7,8] and degradation by Hofmann elimination and S_N2 displacement especially under high temperature and pH [4,9,10]. In the last few years, many efforts have been made to develop AEMs without QA groups [3]. Therein, imidazolium (IM)-based AEMs received much attention, due to their facile fabrication, high hydroxide conductivity, good chemical stability and desired selective solubility [7,11–16]. Nevertheless, the application of IM-based AEMs in H_2/O_2 fuel cell was very limited and the performances reported were far from satisfactory. Zhang et al. [16] used IM-functionalized polysulfone as the AEM and AEI spontaneously in H_2/O_2 fuel cells. The peak power density (P_{max}) of the fuel cell was 16 mW cm^{-2} but the cell performance could last only a few minutes and decayed gradually to zero. Furthermore, Deavin et al. [4] investigated the performances of QA and IM groups on non-aromatic polymer backbone. They found that IM-based and QA-based AEMs showed similar ion exchange capacity and anion conductivity, but the P_{max} of fuel cell utilizing IM-based polymer was only ~1.1 mW cm^{-2} which was far less than that of ~150 mW cm^{-2} for fuel cell having QA-based AEM and AEI. Although Ran et al. [14] reported a P_{max} of 30 mW cm^{-2} could be achieved by using IM-based poly (phenylene oxide) membrane, the ionomer applied in their work was still QA-based polymers. According to the results above, it appears that IM-based polymers are not suitable for the application in AEMFCs. But is it the truth?

On the basis of the literature, the hydroxide conductivity of IM-based membranes can reach as high as that of QA-based membranes, at least 10 mS cm^{-1} at room temperature [4,13,16]. That is, the IM-based membranes meet the conductivity requirement for the fuel cell application [17]. As a result, the poor performance of AEMFCs adopting IM-based AEM and AEI may be resulted from the poor performance of ionomer or the poison effect on the catalyst applied by ionomer. In the electrode, the ionomer directly contacts the catalysts, and whether the groups on the ionomer will deteriorate the activity of catalysts should be well understood. Recently, our group found that imidazole-based ionic liquids were not suitable for the application of PEMFCs, because imidazole-based ionic liquids strongly poisoned the Pt/C catalyst in acidic medium [18]. To date, in the development of AEI, studies of the interaction between AEI and catalysts, and the effect of AEI towards the activity of catalysts has not been reported.

Based on the existing literature, the IM groups of reported AEMs were mainly methyl substituted [4,7,11,13–15]; the effect of the aliphatic substituent group length of IM on the properties of IM-functionalized polymer was, to the best of our knowledge, seldom reported. In addition, as the backbone matrix of the AEM, good chemical stability and mechanical strength are required [7,14]. PES is a well-known engineering polymer with good solubility, thermal stability, chemical resistance and mechanical properties, thus PES is suitable to serve as the backup matrix of AEMs.

Herein, we made use of PES as the polymer backbone to prepare IM-functionalized polymers. The properties of IM-based AEMs can be controlled by the degree of chloromethylation (DCM) of PES. The effect of the alkyl line length of the IM group on the properties of IM-based PES was studied. Furthermore, the influence of IM-based and commercial QA-based AEI on the catalytic activity of Pt/C catalysts towards hydrogen oxidation reaction (HOR) and ORR were evaluated in 0.1 M KOH aqueous solutions. On the basis of the fabricated AEM and AEI, H_2/O_2 AEMFCs with varied ionomer contents in the electrode were assembled, and a P_{max} of ~30 mW cm^{-2} could be yielded at 45 °C, which is as high as that of fuel cell with QA-based ionomer reported by Ran et al. [14], indicating the feasibility of IM-based ionomer in fuel cells.

2. Experimental

2.1. Chloromethylation of PES

Typically, 2 g PES (reduced viscosity = 0.36 dl g^{-1} in N,N-Dimethylformamide (DMF) at 25 °C, produced by Changchun Jilin University Special Plastic Engineering Research) was dissolved into 30 mL ice-cold 98% concentrated H_2SO_4 followed by addition of 5 mL of 1, 4-bis (chloromethoxy) butane (BCMB) (≥95%, Xi'an Langene Bioscience Co. Ltd). Subsequently, the reaction was kept in the ice-water bath for some time and the product was separated by precipitation the mixture in ice water, followed by thorough washing with de-ionized water, and then drying at 50 °C in air. Then the chloromethylated PES (CMPES) was obtained.

2.2. IM-functionalized PES fabrication

For the fabrication of 1-methylimidazole functionalized PES (PES-MeIm), CMPES was dissolved in 1-methylimidazole (>99%, Aladdin) to give a polymer concentration of 5 wt. %, and this polymer solution was stirred at room temperature for 24 h. Then the solution was poured onto a glass plate to cast the membrane and dried in oven at 80 °C for 24 h. The membrane obtained was denoted as PES-MeIm/Cl. The average thickness of PES-MeIm/Cl membrane with different DCM was close (Table S1). Subsequently, the PES-MeIm/Cl membranes were immersed in a 1 M KOH solution for 24 h, converting the membranes from the Cl^- form into the OH^- form (PES-MeIm/OH), followed by washing with de-ionized water several times and storing in de-ionized water for another 48 h to completely remove the residual KOH prior to further experiments.

The procedures for the fabrication of 1-ethylimidazole functionalized PES (PES-EtIm) were the same as that of PES-MeIm, except that 1-methylimidazole was replaced by 1-ethylimidazole (>99%, TCI). For the fabrication 1-butylimidazole functionalized PES (PES-BuIm), 0.4 g CMPES was dissolved in 1-methyl-2-pyrrolidone (NMP) followed by

addition of 1 g 1-butylimidazole (>99%, Alfa Aesar) to give final polymer concentration of 5 wt. %. The other procedures are performed as mentioned above.

2.3. Structure characterization

The DCM for the chloromethylated polymer was determined by ^{1}H NMR spectroscopy on a Bruker Avance II 400 NMR spectrometer at a resonance frequency of 400.13 MHz, using DMSO-d_6 as the solvent and tetramethylsilane (TMS) as an internal standard. The thermal properties of the membranes were tested by using a TGA analyzer (TA Instruments Q500). Before test, the membrane samples were vacuum-dried at 60 °C overnight. Then samples were heated from room temperature to 700 °C at a heating rate of 10 °C min^{-1} under N_2 flow. Derivative thermogravimetry (DTG) curves were obtained by making the first order differential of TGA curve on temperature. The scanning electron microscope (SEM) images and composition of membrane were taken by JEOL JSM-6360LV SEM equipped with Oxford Inca EDX detector. The intrinsic viscosity ([η]) of CMPES in DMF at 25 °C was measured by viscometric method using Ubbelohde viscometer [19].

2.4. Ion exchange capacity, water uptake, swelling ratio and hydroxide ion conductivity

For the measurements of ion exchange capacity (IEC), water uptake (WU) and swelling ratio (SR) of membranes, the OH^- form membranes were dried at 60 °C under vacuum overnight.

The measured IEC (IEC_m) of membranes was determined by the back titration method. Briefly, the dried OH^- form membranes were immersed in 30 mL 0.01 M HCl aqueous solutions for 24 h, followed by back titration of 0.01 M NaOH solution with phenolphthalein as the indicator. The 30 mL 0.01 M HCl solution was used as the blank sample for the control experiment. The IEC_m (mmol g^{-1}) of the membrane was calculated as follows:

$$IEC_m = \frac{(V_b - V_a)c_{HCl}}{m_{dry}} \quad (1)$$

where V_b and V_a were the consumed volumes (mL) of the NaOH solution for the blank sample and the membrane sample, respectively, c_{HCl} was the concentration of HCl solutions (mol l^{-1}), m_{dry} was the mass of dry membrane (g).

The water uptake and swelling ratio of the OH^- form membranes were measured by the following equations:

$$WU = \frac{m_{wet} - m_{dry}}{m_{dry}} \quad (2)$$

$$SR = \frac{l_{wet} - l_{dry}}{l_{dry}} \quad (3)$$

where m_{wet} and m_{dry} were the mass of wet and dry membranes, respectively, l_{wet} and l_{dry} were the average length [$l_{wet} = (a_{wet} \cdot b_{wet})^{1/2}$, $l_{dry} = (a_{dry} \cdot b_{dry})^{1/2}$] of wet and dry membrane samples, respectively, in which, a_{wet}, b_{wet} and a_{dry}, b_{dry} were the lengths and widths of wet and dry membrane samples, respectively.

The ionic conductivity of membrane was measured by a two-probe AC impedance spectroscopy with a Solartron 1260 frequency response analyzer (Solartron Analytical, UK) interfaced with a 1287 potentiostat/galvanostat. The measurement was conducted in the potentiostatic mode over frequencies ranging from 10 MHz to 1 Hz with a potentiostatically controlled AC potential of 20 mV. Ionic conductivity, σ (mS cm^{-1}), was calculated according to the following equation:

$$\sigma = l/wdR \quad (4)$$

where l was the length of the membrane (cm) between two electrode, w and d was the membrane width and thickness, respectively, R was the measured membrane resistance (mΩ).

2.5. Alkaline and oxidative stability testing

The alkaline stability of PES-MeIm/OH membranes was evaluated by monitoring the variation of IEC_m in 2 M KOH at room temperature. After a given time, one piece of membrane was taken out and its IEC_m was measured by the method mentioned above.

The oxidative stability of PES-MeIm/OH membranes was studied by estimating the weight and IEC_m of the membrane in Fenton's reagent. The membrane was immersed into Fenton's reagent (4×10^{-6} mol L^{-1} $FeSO_4$ in 3% H_2O_2) at room temperature. A specific piece of membrane was taken out of the solution after a given time, weighed after removing the surface liquid with filter paper and put into the Fenton's reagent again. Simultaneously, another piece of membrane was taken out and its IEC_m was measured.

2.6. Electrochemical analysis

Electrochemical study was performed at room temperature on CHI 730D electrochemical station (CH Instruments, Inc.) with a rotating disk electrode system in a conventional three electrode electrochemical system. Rotating disk electrode (RDE) with a glassy carbon disk (4 mm in diameter) was used as the working electrode. Saturated calomel electrode (SCE) and Pt foil was used as reference and counter electrode, respectively. The SCE had double salt bridges, and it was taken out from the KOH solution immediately after the measurement so as to minimize the interference of chloride ions from the SCE to the results. Electrolyte was chosen to be 0.1 M KOH aqueous solutions. For experiments with imidazole and tertiary amine containing electrolyte, imidazole or tertiary amine was injected into the electrolyte in order to obtain the given concentration.

Electrocatalysts slurry was prepared as follows: 5 mg 40 wt. % Pt/C (Johnson Matthey) was dispersed in a 2.5 mL mixture of isopropanol and one of the three ionomer solutions including 5 wt. % Nafion solution (DuPont, USA), 5 wt. % AS-4 anion exchange ionomer (Tokayama, Japan) and homemade 2 wt. % PES-EtIm/OH solution in ethanol/water mixture (2/1 vol.). The ionomer added in the electrocatalysts slurry is 16.9 mg, 16.9 mg and 42.3 mg for Nafion, AS-4 and PES-EtIm/OH solution, respectively, in order to give the same

polymer mass for the ionomer. The mixture was sonicated for 20–30 min to form ink, and 6 μL of this ink was dropped on the glassy carbon disk and allowed to dry in air at room temperature.

Before electrochemical test the potential of working electrode was scanned between −1.0 and 0.2 V (vs. SCE) at 100 mV s^{-1} in N_2-purged electrolyte for several times in order to clean the surface of catalysts. The cyclic voltammograms (CVs) of catalysts were recorded in N_2-purged electrolyte at 50 mV s^{-1}. The Pt mass based specific electrochemical surface area (ECSA) is calculated from integrated hydrogen adsorption and desorption cyclic voltammograms using 0.21 mC cm_{Pt}^{-2} as the conversion factor [20]. The ORR polarization curves were recorded positively at a sweep rate of 10 mV s^{-1} in O_2-saturated electrolyte at 1600 rpm. The HOR polarization curves were recorded positively at a sweep rate of 5 mV s^{-1} in H_2-saturated electrolyte at 900 rpm.

The kinetic current of the catalyst for HOR or ORR was calculated by using the well-known mass-transport correction (Koutecky–Levich equation) for rotating disk electrodes: $j^{-1} = j_k^{-1} + j_d^{-1}$ [21], where j is the experimentally obtained current density, j_d is the measured diffusion limiting current density, and j_k the kinetic current density of HOR or ORR. The mass activity towards HOR or ORR was calculated by dividing j_k by the mass of Pt on the RDE.

2.7. H_2/O_2 fuel cell testing

There are two methods (Method A and Method B) for the fabrication of electrode. Method A was performed as follows: The catalyst ink was prepared by ultrasonically blending 50 wt. % Pt/C (Johnson Matthey) electrocatalysts powder with homemade PES-EtIm/OH AEI and isopropanol for 30 min at different catalyst/ionomer weight ratio. The catalyst ink was then sprayed onto a wet-proofed carbon gas diffusion layer (GDL) on the hot plate at 60 °C. For Method B, catalyst and ionomer was sprayed separately, that is, catalysts were firstly sprayed onto the GDL followed by the spray of ionomer. The other procedures were the same as that of Method A. The Pt loading for all electrodes was 0.4 mg_{Pt} cm^{-2}.

The water on the surface of PES-MeIm/OH membrane (40–50 μm in thickness) was absorbed by filter papers before use. The MEAs with an active area of 5 cm^2 were fabricated by hot-pressing the anode and cathode electrodes on both sides of a PES-MeIm/OH membrane at 60 °C for 2 min. The MEA was then cooled and assembled in 5 cm^2 single cells for testing.

The single cell testing was conducted at 45 °C with fully humidified H_2 and O_2 under 150 kPa_{abs} for the anode and cathode, respectively. The flow rate for H_2 and O_2 was 50 and 100 mL min^{-1}, respectively. Both the polarization curves and the internal ohmic resistance of the fuel cell (at 10 kHz) were measured by Kikusui KFM-2030 FC Impedance Meter at the same time.

The cyclic voltammetry (CV) curve of electrode in the fuel cell was recorded on CHI-600C (CH Instruments, Inc.) at 30 °C with the other electrode as the count and reference electrode (dynamic hydrogen electrode, DHE), and the target electrode was cycled between 0 and 1.0 V (vs. DHE) at a sweep rate of 20 mV s^{-1}, using fully humidified H_2 at the other electrode and dry N_2 at the target electrode. The region corresponding to hydrogen desorption region was used to measure the electrochemical active area of the target electrode, using 0.21 mC cm_{Pt}^{-2} as the conversion factor.

3. Results and discussion

3.1. Chloromethylation of PES

The chloromethylation of PES was carried out using 1, 4-bis (chloromethoxy) butane (BCMB) as the chloromethylating reagent and concentrated H_2SO_4 as the solvent and catalyst (Fig. 1). BCMB is a kind of high-efficient, non-carcinogenic and inexpensive chloromethylating reagent, thus the commonly used carcinogenic chloromethyl methyl ether was avoided.

The chemical structures of PES and CMPES are analyzed using ^1H NMR spectrum and the corresponding spectra are shown in Fig. 2. The hydrogen atoms in the polymer are denoted as H_x, where x represents the position marked in

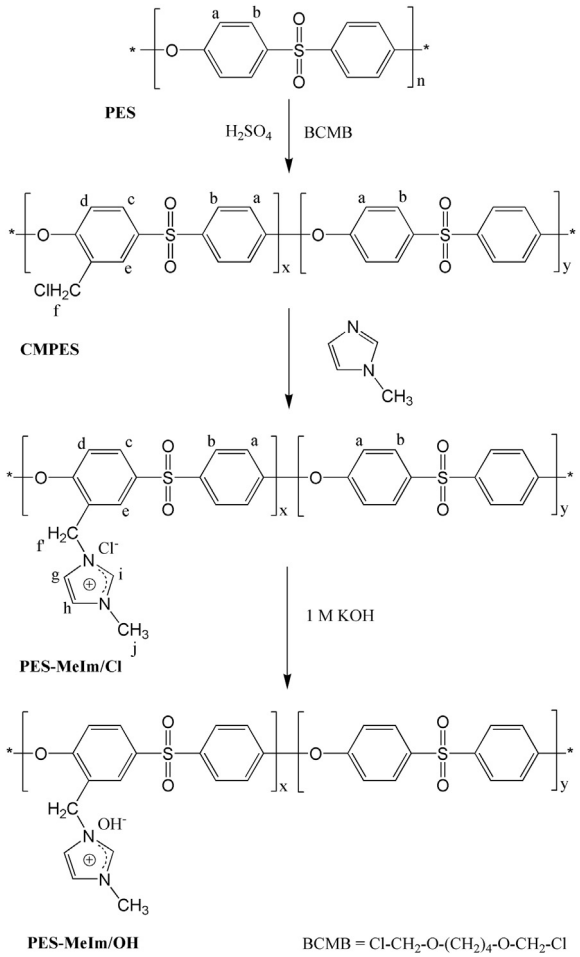

Fig. 1 – Synthesis of PES-MeIm/OH.

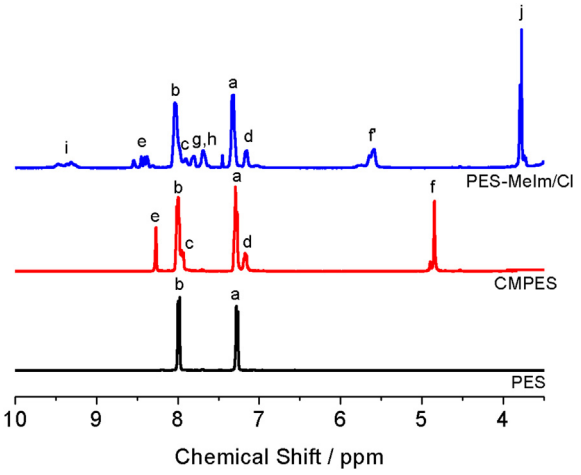

Fig. 2 – ^{1}H NMR spectra of PES, CMPES and PES-MeIm/Cl.

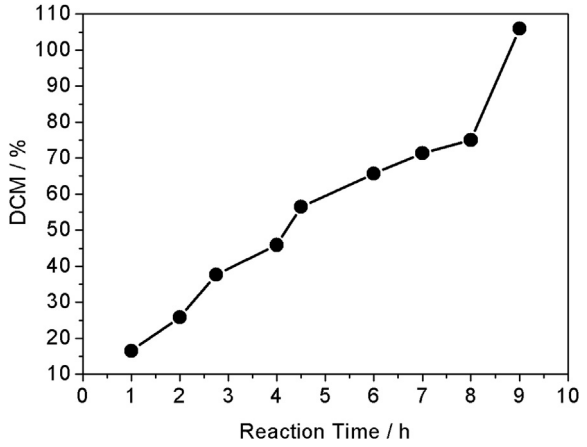

Fig. 3 – The relationship between DCM of CMPES and reaction time.

Fig. 1. For the pristine PES, there are only two groups of peaks around 8.0 ppm and 7.3 ppm, respectively, which are attributed to the H_b and H_a atoms in aromatic rings. After chloromethylation, a new couple of peaks appear around 4.85 ppm, which come from H atoms in chloromethyl groups [7,12,22], confirming the chloromethylated polymer has been successfully synthesized. As an electrophilic substitution, the reaction of polymers would preferentially take place in the benzene rings next to the ether bond due to the highest electron-density [12]. Accordingly, the new peaks around 8.3, 7.9 and 7.1 can be assigned to the H atoms in the aromatic rings where chloromethyl groups grafted. In contrast, due to the strong electron-withdrawing effect of the sulfone group, the H_b atoms possess the lowest electron-density, resulting in the inertness of electrophilic substitution during the chloromethylation reaction. Therefore, the degree of chloromethylation (DCM) of PES, defined as the average number of chloromethyl groups per repeat unit of PES, can be calculated by the following equation: $DCM = 2A(H_f)/[A(H_b) + A(H_c) + A(H_e)]$, where $A(H_f)$, $A(H_b)$, $A(H_c)$ and $A(H_e)$ are the integrated area of the corresponding peaks on the ^{1}H NMR spectra. In addition, owing to the low reaction temperature, the sulfonation of polymers was avoided [12].

The degree of chloromethylation (DCM) of chloromethylated polymers is an important parameter, which determines the IEC_m and mechanical properties of the resulting AEMs. In this study, DCM can be controlled by varying the chloromethylation time (Fig. 3). As shown in Fig. S1, the $A(H_f)$ of the CMPES increases with the chloromethylation time, which reflects the increase of DCM. Moreover, it was found that the $[\eta]$ of CMPES rose with the increase of DCM (Table 1), which is consistent with the previous study results [19].

3.2. *Structure characterization of 1-methylimidazole functionalized PES*

The PES-MeIm/Cl was obtained by the Menshutkin reaction between 1-methylimidazole and chloromethyl groups [7]. After Menshutkin reaction, the ^{1}H NMR spectrum (Fig. 2) shows that the peaks at 4.85 ppm (H_f) shift to lower magnetic field at 5.59 and 5.64 ppm ($H_{f'}$), meanwhile, new signals arise at around 3.7, 7.7 and 9.4 ppm, which can be ascribed to the H atoms on the imidazolium. The change of ^{1}H NMR spectrum confirmed the complete conversion of chloromethyl groups and successful synthesis of PES-MeIm/Cl. After alkalization in 1 M KOH for 24 h, PES-MeIm/Cl was converted to PES-MeIm/OH. The cross-sectional and surface SEM images of PES-MeIm/OH shown in Fig. S2 indicate the compactness of the membrane, which is beneficial for the fuel cell application because the gas-impermeability is required.

The thermal degradation of PES, CMPES and PES-MeIm/OH were investigated using thermogravimetric (TG) analysis between room temperature and 700 °C under N_2 protection. As shown in Fig. 4, PES is thermal stable before polymer main-chain decomposition starting at around 450 °C. For CMPES, there are three weight loss stages: the first one starts at around 150 °C, which may be attributed to the release of chlorine-containing compounds (e.g., HCl or Cl_2) arising from crosslinking of the chloromethyl groups with aromatic rings [12]; the second stage is due to the removal of the methylene groups formed by the previous crosslinking [12]; and the third stage comes from the main-chain decomposition. For PES-MeIm/OH, the weight loss below 150 °C is owing to the removal of the residual water bound with the imidazolium groups. The decomposition of imidazolium groups commences at around 160 °C, which is close to the decomposition temperature reported for imidazolium functionalized polysulfones and poly(phenylene oxide) membranes [14,16]. With the increase of temperature, the degradation of residual groups of the degraded imidazolium groups and main-chain commences in succession, which give rise to the next two weight loss steps.

3.3. *IEC_m, water uptake, swelling ratio, hydroxide conductivity and stability of PES-MeIm/OH*

Generally, the IEC_m of AEMs is determined by the DCM of chloromethylated polymer matrix. As expected, the IEC_m of

Table 1 – Degree of chloromethylation and intrinsic viscosity of CMPES; IEC_m, water uptake, swelling ratio and hydroxide conductivity of PES-MeIm/OH membranes.

Membrane	DCM %	$[\eta]$[a] dl g^{-1}	IEC_m mmol g^{-1}	WU %	SR %	σ mS cm^{-1}
PES-MeIm/OH-#1	25.8	0.3918	0.56	18.8	7.5	1.8
PES-MeIm/OH-#2	45.9	0.4067	0.91	38.7	18.5	6.6
PES-MeIm/OH-#3	56.5	0.4579	1.25	55.1	25.0	7.4
PES-MeIm/OH-#4	65.7	0.4843	1.54	67.6	32.4	14.9
PES-MeIm/OH-#5	75.0	0.4941	1.65	120.0	46.2	9.6
PES-MeIm/OH-#6	105.8	0.5101	n.a.	n.a.	n.a.	n.a.

a Intrinsic viscosity of CMPES in DMF at 25 °C.

PES-MeIm/OH rises with the increase of DCM (Table 1). Moreover, the EDX spectra of CMPES and PES-MeIm/OH shown in Fig. S3 indicated that peaks corresponding to Cl element completely disappeared after 1-methylimidazole and KOH treatment, confirming the sufficient conversion of $-CH_2Cl$ and alkalization. The properties of AEMs, such as WU, SR and hydroxide conductivity are affected significantly by the IEC_m. With the increase of IEC_m, the density of the hydrophilic ion exchange groups increases and the water transfer channels become more continuous [17], resulting in the fact that more water can be adsorbed. As shown in Table 1, the WU remarkably increases from 18.8% for PES-MeIm/OH-#1 (IEC_m = 0.56 mmol g^{-1}) to 120.0% for PES-MeIm/OH-#5 (IEC_m = 1.65 mmol g^{-1}). For the uncrosslinked PES-MeIm/OH membranes, the more water the membrane uptakes, the higher degree of swelling the membrane shows, thus the SR of these PES-MeIm/OH membranes also rises with IEC_m and WU. For the CMPES with DCM = 105.8%, the IM-functionalized membrane (PES-MeIm/Cl-#6) directly dissolved in water, so the properties of this membrane cannot be measured.

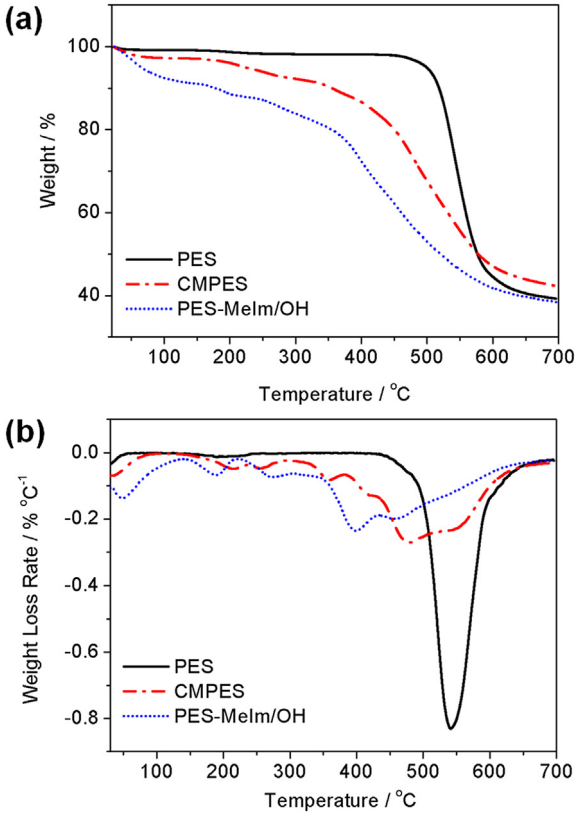

Fig. 4 – (a) TGA and (b) DTG curves of PES, CMPES and PES-MeIm/OH.

The hydroxide conductivity of PES-MeIm/OH membrane was determined by the hydroxide concentration and the hydroxide transport ability of membranes. With the IEC_m increases from 0.56 to 1.54 mmol g^{-1}, the hydroxide conductivity continuously increases, reaching 14.9 mS cm^{-1} for PES-MeIm/OH-#4, which is close to the hydroxide conductivity of the imidazolium-based AEMs reported in literature (Table 2). Interestingly, the PES-MeIm/OH-#5 possessed the greatest IEC_m, but its hydroxide conductivity was lower than that of PES-MeIm/OH-#4. That may be caused by the lower ionic concentration in the membrane, resulting from the significant swelling ratio (46.2%). It was reported by Pan et al. [17] that the conductivity of the AEM was determined by the practical ionic concentration in the membrane which was affected by not only IEC_m but also SR. The practical ionic concentration showed positive relationship with IEC_m but negative relationship with SR. As a result, the practical ionic concentration under measurement conditions may be evaluated by the quotient of IEC_m divided by SR (IEC_m/SR). The relationships of hydroxide conductivity and IEC_m/SR to IEC_m are plotted in Fig. 5. It is found that the variation of hydroxide conductivity is consistent with that of IEC_m/SR; and PES-MeIm/OH-#4 exhibits the highest IEC_m/SR, which in turn gives rise to the greatest hydroxide conductivity. Therefore, IEC_m/SR can be served as an indirect indicator of the ionic concentration in the water-saturated membrane.

Furthermore, the relationship between hydroxide conductivity and temperature was studied (Fig. S4). Obviously, high temperature facilitates the transport of hydroxide, thus the hydroxide conductivity increases with the temperature, reaching ~30 mS cm^{-1} for PES-MeIm/OH-#4 at 80 °C.

The alkaline stability is another important index in the development of AEMs. In this study, the alkaline stability of PES-MeIm/OH-#4 was evaluated by monitoring the variation of IEC_m in 2 M KOH at room temperature. As shown in Fig. 6, no obvious loss of IEC_m is found after 400 h, suggesting the acceptable durability of this IM-functionalized membrane.

The oxidative stability of PES-MeIm/OH-#4 was estimated by monitoring the mass loss of membrane sample in

Table 2 – Comparison of properties of IM-type anion exchange membranes and the corresponding H_2/O_2 fuel cell performance in this work and literature.

Polymer matrix	IEC_m mmol g^{-1}	Hydroxide conductivity[a] mS cm^{-1}	P_{max}[b] mW cm^{-2}	Pt loading mg_{Pt} cm^{-2}	Ionomer	Reference
Poly (ether sulfone)	1.54	14.9	29.5 (45 °C, 150 kPa)[c]	0.4	PES-EtIm/OH	This work
Poly(phenylene oxide)	1.51	9	~30 (50 °C, 100 kPa)	0.4	TMHDA[d] crosslinked PVBC[e]	[14]
Polysulfone (PSF)	1.39 ± 0.27	16.1 ± 2.9	~16 (60 °C, 200 kPa)	2	IM-functionalized PSF	[16]
ETFE-g-PVBC	1.77 ± 0.03	~6[f]	~1.1 (50 °C, 100 kPa)	0.4 ± 0.02	IM-functionalized ETFE-g-PVBC	[4]
Polysulfone	1.35	~15	n.a.	n.a.	n.a.	[7]
Poly(styrene-co-acrylonitrile)	1.58	~12	n.a.	n.a.	n.a.	[13]

a Measured at room temperature in water.
b Peak power density.
c Temperature and absolute gas pressure at fuel cell wording condition.
d TMHDA = N, N, N′, N′-tetramethylhexane-1,6-diamine.
e PVBC = Poly(vinylbenzyl chloride).
f Calculated from the HCO_3^- values using a 3.8 × multiplication factor at 30 °C.

Fenton's reagent (Fig. 7). This method is commonly used in the accelerated durability test of proton exchange membrane for PEMFCs [8,23], and it is now also adopted in the development of AEMs [24,25]. After treatment in Fenton's reagent for ~200 h, the weight loss of PES-MeIm/OH-#4 was only 13% (Fig. 7a). In addition, the IEC_m of the PES-MeIm/OH-#4 was monitored during the treatment. As shown in Fig. 7b, the IEC_m decreased gradually to 0.93 mmol g^{-1} after ~200 h, indicating the degradation of IM groups induced by Fenton's reagent.

3.4. *Comparison of different IM groups*

In order to investigate the effect of the type of IM groups on the properties of IM-based AEMs, the 1-ethylimidazole and 1-butylimidazole were used to functionalize the CMPES with DCM = 65.7%. As shown in the ^1H NMR spectra (Fig. 8), all hydrogen atoms can be well assigned, clearly proving the successful synthesis of PES-EtIm/Cl and PES-BuIm/Cl membranes. After alkalization, PES-EtIm/OH and PES-BuIm/OH were obtained and the physical properties are listed in Table 3.

Taking PES-MeIm/OH-#4, PES-EtIm/OH and PES-BuIm/OH into consideration, it can be found that the WU and SR increases with the elongation of alkyl groups on the IM ring, whereas the hydroxide conductivity gradually declined. That may be explained as follows: the interaction between two polymer lines is weakened with the increase of alkyl groups due to the space effect, that is, the compactness of the membrane become looser, which give rise to the higher WU and larger SR for PES-EtIm/OH and PES-BuIm/OH. In turn, the high WU leads to the low IEC_m/SR, thus the hydroxide conductivity of PES-Im/OH decreases with the elongation of alkyl line on the IM ring.

In this work, the solubility of three IM-type membranes, including PES-MeIm/OH-#4, PES-EtIm/OH and PES-BuIm/OH, were studied. Ethanol and isopropanol were used as the

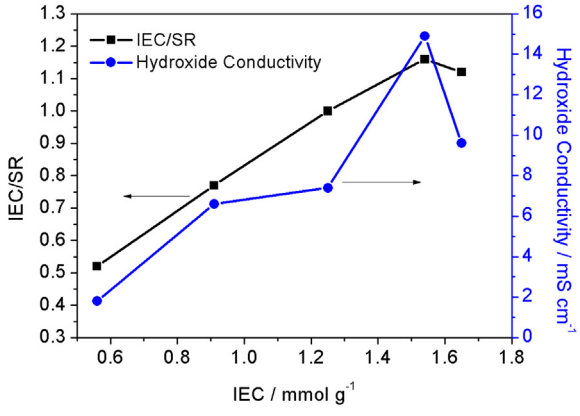

Fig. 5 – The relationships of IEC_m/SR and hydroxide conductivity versus IEC_m for PES-MeIm/OH.

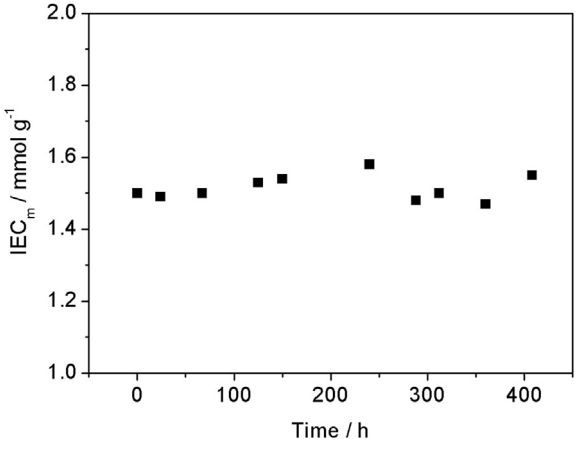

Fig. 6 – The variation of IEC_m of PES-MeIm/OH-#4 as a function of exposure time in 2 M KOH.

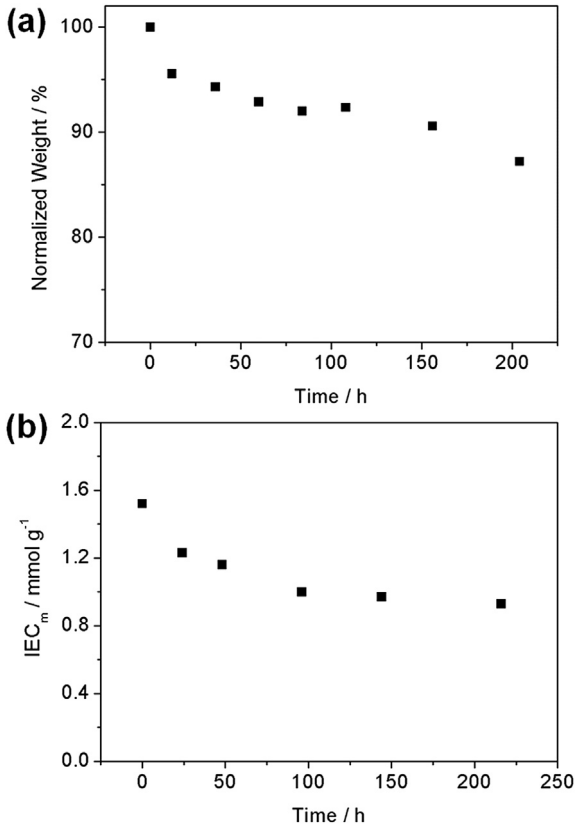

Fig. 7 – (a) Residual weight and (b) IEC_m variation of PES-MeIm/OH-#4 under Fenton's reagent treatment.

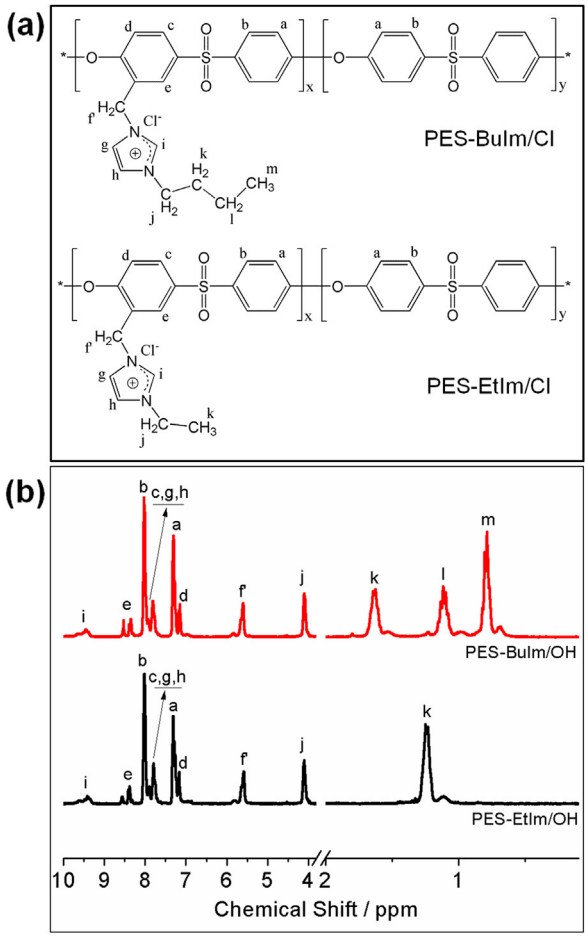

Fig. 8 – (a) The chemical structures and (b) ^{1}H NMR spectra of PES-EtIm/Cl and PES-BuIm/Cl.

solvents due to their wide application and low toxicity. As shown in Table S2, at the ionomer concentration of 2 wt. %, all three membranes cannot dissolve in pure ethanol, isopropanol and water. Fortunately, PES-EtIm/OH and PES-BuIm/OH are able to dissolve in the mixture of ethanol and water after treatment at 70 °C for several minutes and the ionomer solution was stable after cooling down to room temperature. The PES-BuIm/OH could also dissolve in the mixture of isopropanol and water. In comparison, the PES-MeIm/OH-#4 membrane cannot dissolve in the mixture of alcohol and water, even heating at 70 °C for 12 h, which may be due to the stronger interaction among polymer lines than that of PES-EtIm/OH and PES-BuIm/OH as discussed above. The above results suggested that the solubility of IM-functionalized PES was enhanced with the elongation of alkyl substituent group of IM group. In the sight of performance, it is more suitable for PES-EtIm/OH to be used in fuel cells owing to its higher hydroxide conductivity and lower SR than that of PES-BuIm/OH.

3.5. *Electrochemical study of the influence of IM-based AEI on the catalytic reaction of Pt/C catalysts in alkaline medium*

In addition to the high hydroxide conductivity, an ionomer should not poison the catalyst or deteriorate the activity of catalysts. Herein, the effect of IM-based and QA-based ionomer on the activity of Pt catalysts towards HOR and ORR in alkaline medium was studied.

It is well known that the QA-based and IM-based polymers are usually synthesized by the reaction between tertiary amine and imidazole with chloromethyl groups. Before the study of QA-based and IM-based polymers, the effect of tertiary amine and imidazole on the catalysts was evaluated. As shown in Fig. 9a, the pristine CV curve of Pt/C in 0.1 M KOH shows typical hydrogen adsorption/desorption region (from −1.0 V to −0.4 V) and surface oxidation/reduction region (from −0.5 to 0.2 V) [20,26]. After 1-methylimidazole was added into the solution, the CV curve of Pt/C was obviously changed, which may be caused by the significant adsorption of 1-methylimidazole on the surface of platinum, and thus the hydrogen adsorption/desorption and the surface oxidation/reduction peaks are difficult to take place [20]. The effect of 1-methylimidazole on the ORR activity of Pt was shown in Fig. 9b. It can be seen that the ORR activity of Pt was deteriorated severely in the presence of 1-methylimidazole and the degradation degree was positively correlated with the concentration of 1-methylimidazole. In contrast, 1-methylimidazole has little adverse influence on the HOR performance of Pt (Fig. 9c). These results indicate that the strong adsorption of 1-methylimidazole on the surface of Pt

Table 3 – Degree of chloromethylation, IEC_m, water uptake, swelling ratio and hydroxide conductivity of PES-EtIm/OH and PES-BuIm/OH membranes.

Membrane	DCM %	IEC_m mmol g^{-1}	WU %	SR %	IEC/SR	Hydroxide conductivity mS cm^{-1}
PES-EtIm/OH	65.7	1.54	167.0	55.1	0.99	13.5
PES-BuIm/OH		1.56	179.5	63.3	0.95	5.4

blocked the active sites of ORR, whereas the HOR was not affected. The influence of tertiary amine on the electrochemical performances of Pt was also studied. We chose triethylamine (TEA) as the targets instead of trimethylamine (TMA), because TEA is less volatilizable than that of TMA. As shown in Fig. 9d, the addition of TEA to the electrolyte also decrease the ECSA of Pt, and a new peak appeared at around −0.35 V which may come from the oxidation of TEA on the surface of Pt [27]. Moreover, the ORR activity of Pt was decreased by TEA as that of 1-methylimidazole, but the degradation degree was smaller (Fig. 9e). Similarly, the HOR performance of Pt was slightly interfered except that the oxidation of TEA also takes place in the presence of hydrogen (Fig. 9f).

Furthermore, the electrochemical performances of Pt/C in the presence of IM-based AEI (PES-EtIm/OH) and QA-based AEI (AS-4) were studied. AS-4 is a commercially available QA-based ionomer, and it performed well in the electrode of AEMFCs [28]. For the sake of comparison, Nafion ionomer is used as the baseline, because Nafion is commonly utilized for the RDE measurement not only in acidic but also in alkaline medium [29,30]. As shown in Fig. 10a and b, the ECSA of Pt/C in the presence of Nafion is $79.4 \pm 2.4\ m^2\ g_{Pt}^{-1}$, which is higher than that of AS-4 ($61.7 \pm 1.7\ m^2\ g_{Pt}^{-1}$) and PES-EtIm/OH ($68.8 \pm 1.5\ m^2\ g_{Pt}^{-1}$). The Pt mass activity towards ORR at −0.05 V for Nafion, AS-4 and PES-EtIm/OH bonded Pt/C was 14.8 ± 2.4, 10.4 ± 1.1, 11.1 ± 1.1 mA mg_{Pt}^{-1}, respectively (Fig. 10c and d). The lower ECSA and ORR activity of Pt/C in the presence of AEI may result from the adsorption of QA and IM groups on the surface of Pt. According to the results above, the 1-methylimidazole and TEA are site blockers to ORR. After the transformation to IM and QA groups, the poisoning effect may be weakened, but can still influence the ORR activity of catalysts. In contrast, Fig. 10e and f present that the HOR mass activity of Pt at −0.98 V in the presence of AS-4 and PES-EtIm/OH is 294.9 ± 18.5 and $333.5 \pm 11.3\ m^2\ g_{Pt}^{-1}$, respectively, both of which are higher than that of Nafion ($190.4 \pm 6.1\ m^2\ g_{Pt}^{-1}$), suggesting that the HOR was not negatively affected by IM and QA ionomers. These results above indicate that the IM-based AEI does not have more adverse effects on the activity of Pt/C catalysts than QA-based ionomers. Additionally, the CV curve of PES-EtIm/OH shows that there are no obvious redox couples on PES-EtIm/OH ionomer (Fig. S5), indicating its stability under the potential range where electrochemical reactions occur. As a result, the IM-based PES-EtIm/OH ionomer may have potential application in AEMFCs.

3.6. H_2/O_2 fuel cell performance

The effect of ionomer content in the electrodes on the performance of H_2/O_2 fuel cells with PES-MeIm/OH-#4 membranes was studied using fully humidified H_2 and O_2. According to the literature, many researchers settled the working temperature of AEMFCs below 50 °C [14,31,32]; the fuel cells in this work were tested at 45 °C. As shown in

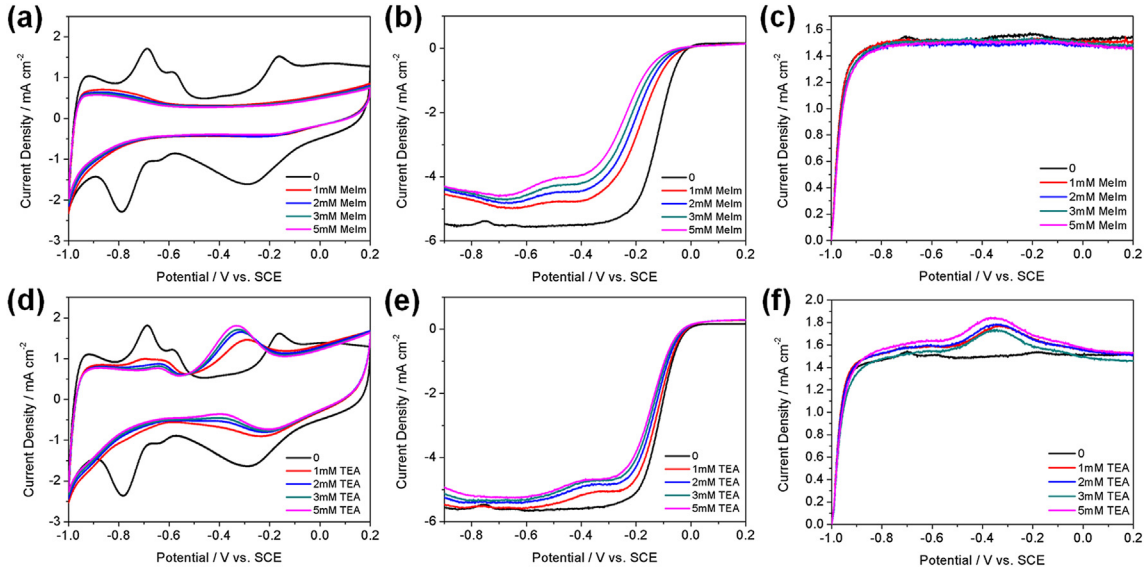

Fig. 9 – (a) CV, (b) ORR and (c) HOR curves of Pt/C in 0.1 M KOH containing different concentration of 1-methylimidazole; (d) CV, (e) ORR and (f) HOR curves of Pt/C in 0.1 M KOH containing different concentration of TEA. The catalyst binder used is Nafion.

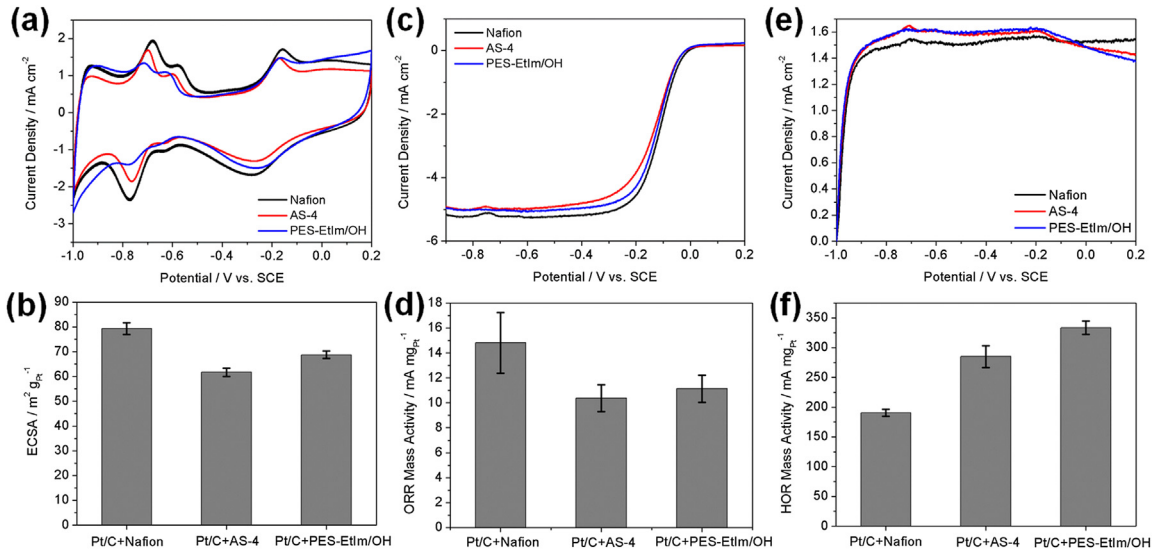

Fig. 10 – (a) CV, (c) ORR and (e) HOR curves of Pt/C in the presence of Nafion, PES-EtIm/OH and AS-4. (b) ECSA, (d) ORR mass activity at −0.05 V and (f) HOR mass activity at −0.98 V for Pt/C in the presence of Nafion, PES-EtIm/OH and AS-4.

Table 4, the open circuit potential of all AEMFCs is above 1.0 V except FC-#1, indicating that the Pt/C catalysts are not poisoned. The weight ratio between the ionomer and catalyst, denoted as I:C, was found to have a significant impact on the performance of fuel cells. As presented in Fig. 11, the performance of fuel cell is quite poor at very low ionomer content (FC-#1). With the increase of ionomer content, the P_{max} increases, reaching 22.5 mW cm^{-2} at I:C = 3:7 (FC-#3). It is considered that higher content of ionomer gives rise to more three-phase boundaries in the electrode and easier transport of hydroxide, which is confirmed by the reduction of internal ohmic resistance of fuel cells (Table 4). Further increase of ionomer content to I:C = 4:6 (FC-#4) will not improve the fuel cell performance, which may result from the block of the electron pathway and active sites of catalysts by the excessive ionomer.

The fabrication method of electrode was also evaluated. When the anode was prepared by Method B, the P_{max} of fuel cell (FC-#5) was enhanced to 29.5 mW cm^{-2} in comparison with FC-#3 (Table 4 and Fig. 11). The CV curves of anode of FC-#3 and FC-5# were shown in Fig. 11c. The electrochemical active area for the anode of FC-#3 and FC-#5 was calculated to be 84.4 and 84.3 cm^2_{pt} cm^{-2}_{geo}, respectively, indicating that the difference of performance between FC-#3 and FC-#5 should not come from the difference of active catalytic area. As a result, it was considered that the higher performance of FC-#5 may be ascribed to the reduced interacting resistance at the interface of membrane and anode, because the ionomer of anode is sprayed separately before the MEA was hot pressed, which is reflected from the reduced internal ohmic resistance for FC-#5 than FC-#3 (Table 4). Moreover, the higher concentration of the unoccupied surface catalytic sites for HOR in FC-#5 than that of FC-3# may be another reason for the grater P_{max} of FC-#5. It was suggested previously that the occupation of anodic catalyst surface by the electro-generated water is probably one of the main causes leading to the low AEMFC performance [33]. Therefore, the water should be removed effectively in order to guarantee the smooth oxidation of hydrogen. It has been found that the electrode fabricated by the ionomer impregnation method (like Method B in this work) had improved ability of draining off water compared with electrode made by thin-film method (Method A) [34]. As expected, the fuel cell (FC-#5) using anode made by Method B presented higher P_{max} than that of the FC-#3.

Table 4 – The P_{max}, open circuit potential and internal ohmic resistance of fuel cells with different electrodes.

Fuel cell	Ionomer:catalyst (weight ratio)	Preparation method		P_{max} mW cm^{-2}	Open circuit potential V	Internal ohmic resistance[a]
		Anode	Cathode			mΩ
FC-#1	1:9	Method A	Method A	0.81	0.927	n.a.[b]
FC-#2	2:8	Method A	Method A	7.1	1.011	323.7
FC-#3	3:7	Method A	Method A	22.5	1.015	114.2
FC-#4	4:6	Method A	Method A	21.0	1.013	114.1
FC-#5	3:7	Method B	Method A	29.5	1.010	107.4

a Measured at open circuit potential.
b Cannot measure.

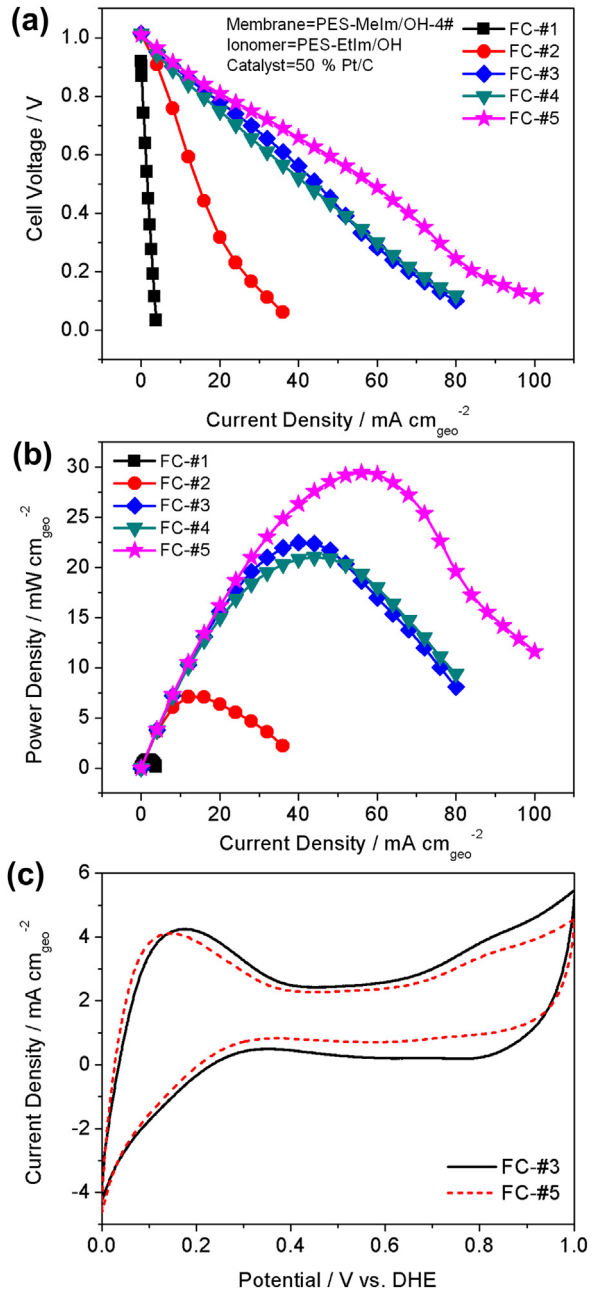

Fig. 11 – (a) Polarization curves and (b) power density curves of H_2/O_2 fuel cells with different electrodes at 45 °C. (c) CV curves of the anode of FC-#3 and FC-#5.

The P_{max} in this work (29.5 mW cm^{-2}) is close to the recent reported P_{max} of 30 mW cm^{-2} on the fuel cell with IM-type poly(phenylene oxide) membrane [14], but the ionomer used in that report was QA-based. More impressively, the value of 29.5 mW cm^{-2} is much better than the P_{max} of ~16 mW cm^{-2} [16] and ~1.1 mW cm^{-2} [4] reported previously using IM-type AEM and AEI in the fuel cell (Table 2). Although many parameters in the MEA preparation, such as catalyst ink components, electrode preparation method and hot-pressing temperature, need to be optimized, the IM-based membrane and ionomer are proved to be a candidate which are worth further investigation for the application in the AEMFCs.

4. Conclusions

This study reports the development of IM-based AEMs synthesized by functionalization of chloromethylated PES with 1-methylimidazole, 1-ethylimidazole and 1-butylimidazole. The properties of IM-functionalized AEMs can be controlled by the DCM of PES. With the elongation of alkyl line on the IM groups, the hydroxide conductivity of AEM decreased, but the solubility was improved. As a result, the IM-based AEIs could be obtained in the mixture of ethanol and water. Moreover, it was found that IM-based AEI only had minor adverse effect on the activities of Pt/C catalysts towards HOR and ORR, which was important for the application of AEI in fuel cells. A single fuel cell employing IM-based AEM and AEI yielded a P_{max} of 29.5 mW cm^{-2} at 45 °C, revealing the feasibility of IM-functionalized polymer in the AEMFC. In addition, other ionomer and membrane properties remain to be determined including hydrogen and oxygen permeability, which is an important parameter for the AEMs used for fuel cells. The further investigation should be focused on improving the conductivity of membrane and enhancing the chemical resistance to hydroxyl radicals, low relative humidities and higher operating temperatures. The strategies applied in the development of proton exchange membrane may be used for reference. For example, phase separation structure in the membrane is expected to increase the conductivity of membrane with relatively low water uptake, and the addition of free radical quenchers will probably improve the oxidation stability, and the incorporation of hydrophilic metal oxide may enhance the performance under low relative humidities and higher operating temperatures.

Acknowledgments

This work was financially supported by the National High Technology Research and Development Program of China (863 Program, No. 2011AA050705), National Basic Research Program of China (973 Program, No. 2012CB215500) and the National Natural Science Foundations of China (No. 20936008, No. 21076208).

Appendix A. Supplementary data

Supplementary data related to this article can be found at http://dx.doi.org/10.1016/j.ijhydene.2013.05.070.

REFERENCES

[1] Wang Y, Chen KS, Mishler J, Cho SC, Adroher XC. A review of polymer electrolyte membrane fuel cells: technology, applications, and needs on fundamental research. Appl Energy 2011;88:981–1007.
[2] Bing YH, Liu HS, Zhang L, Ghosh D, Zhang JJ. Nanostructured Pt-alloy electrocatalysts for PEM fuel cell oxygen reduction reaction. Chem Soc Rev 2010;39:2184–202.
[3] Couture G, Alaaeddine A, Boschet F, Ameduri B. Polymeric materials as anion-exchange membranes for alkaline fuel cells. Prog Polym Sci 2011;36:1521–57.

[4] Deavin OI, Murphy S, Ong AL, Poynton SD, Zeng R, Herman H, et al. Anion-exchange membranes for alkaline polymer electrolyte fuel cells: comparison of pendent benzyltrimethylammonium- and benzylmethylimidazolium-head-groups. Energy Environ Sci 2012;5:8584–97.
[5] Matsumoto K, Fujigaya T, Yanagi H, Nakashima N. Very high performance alkali anion-exchange membrane fuel cells. Adv Funct Mater 2011;21:1089–94.
[6] Merle G, Wessling M, Nijmeijer K. Anion exchange membranes for alkaline fuel cells: a review. J Membr Sci 2011;377:1–35.
[7] Yan XM, He GH, Gu S, Wu XM, Du LG, Wang YD. Imidazolium-functionalized polysulfone hydroxide exchange membranes for potential applications in alkaline membrane direct alcohol fuel cells. Int J Hydrog Energy 2012;37:5216–24.
[8] Zhao D, Li JH, Song MK, Yi BL, Zhang HM, Liu ML. A durable alternative for proton-exchange membranes: sulfonated poly(benzoxazole thioether sulfone)s. Adv Energy Mater 2011;1:203–11.
[9] Tanaka M, Fukasawa K, Nishino E, Yamaguchi S, Yamada K, Tanaka H, et al. Anion conductive block poly(arylene ether)s: synthesis, properties, and application in alkaline fuel cells. J Am Chem Soc 2011;133:10646–54.
[10] Zhang QA, Zhang QF, Wang JH, Zhang SB, Li SH. Synthesis and alkaline stability of novel cardo poly(aryl ether sulfone)s with pendent quaternary ammonium aliphatic side chains for anion exchange membranes. Polymer 2010;51:5407–16.
[11] Li W, Fang J, Lv M, Chen CX, Chi XJ, Yang YX, et al. Novel anion exchange membranes based on polymerizable imidazolium salt for alkaline fuel cell applications. J Mater Chem 2011;21:11340–6.
[12] Lin BC, Qiu LH, Qiu B, Peng Y, Yan FA. Soluble and conductive polyfluorene ionomer with pendant imidazolium groups for alkaline fuel cell applications. Macromolecules 2011;44:9642–9.
[13] Qiu B, Lin BC, Qiu LH, Yan F. Alkaline imidazolium- and quaternary ammonium-functionalized anion exchange membranes for alkaline fuel cell applications. J Mater Chem 2012;22:1040–5.
[14] Ran J, Wu L, Varcoe JR, Ong AL, Poynton SD, Xu TW. Development of imidazolium-type alkaline anion exchange membranes for fuel cell application. J Membr Sci 2012;415:242–9.
[15] Lin BC, Qiu LH, Lu JM, Yan F. Cross-linked alkaline ionic liquid-based polymer electrolytes for alkaline fuel cell applications. Chem Mat 2010;22:6718–25.
[16] Zhang FX, Zhang HM, Qu C. Imidazolium functionalized polysulfone anion exchange membrane for fuel cell application. J Mater Chem 2011;21:12744–52.
[17] Pan J, Chen C, Zhuang L, Lu JT. Designing advanced alkaline polymer electrolytes for fuel cell applications. Acc Chem Res 2012;45:473–81.
[18] Ke CC, Li J, Li XJ, Shao ZG, Yi BL. Protic ionic liquids: an alternative proton-conducting electrolyte for high temperature proton exchange membrane fuel cells. RSC Adv 2012;2:8953–6.
[19] Ioan S, Filimon A, Avrarn E. Influence of the degree of substitution on the solution properties of chloromethylated polysulfone. J Appl Polym Sci 2006;101:524–31.
[20] Sarkar A, Zhu X, Nakanishi H, Kerr JB, Cairns EJ. Investigation into electrochemical oxygen reduction on platinum in tetraethylammonium hydroxide and effect of addition of imidazole and 1,2,4-triazole. J Electrochem Soc 2012;159:F628–34.
[21] Gasteiger HA, Kocha SS, Sompalli B, Wagner FT. Activity benchmarks and requirements for Pt, Pt-alloy, and non-Pt oxygen reduction catalysts for PEMFCs. Appl Catal B Environ 2005;56:9–35.
[22] Zhang HW, Zhou ZT. Alkaline polymer electrolyte membranes from quaternized poly(phthalazinone ether ketone) for direct methanol fuel cell. J Appl Polym Sci 2008;110:1756–62.
[23] Zhao D, Yi BL, Zhang HM, Liu ML. The effect of platinum in a Nafion membrane on the durability of the membrane under fuel cell conditions. J Power Sources 2010;195:4606–12.
[24] Shen K, Pang J, Feng S, Wang Y, Jiang Z. Synthesis and properties of a novel poly(aryl ether ketone)s with quaternary ammonium pendant groups for anion exchange membranes. J Membr Sci 2013;440:20–8.
[25] Zhang YM, Fang J, Wu YB, Xu HK, Chi XJ, Li W, et al. Novel fluoropolymer anion exchange membranes for alkaline direct methanol fuel cells. J Colloid Interface Sci 2012;381:59–66.
[26] Schmidt TJ, Stamenkovic V, Ross PN, Markovic NM. Temperature dependent surface electrochemistry on Pt single crystals in alkaline electrolyte – part 3. The oxygen reduction reaction. Phys Chem Chem Phys 2003;5:400–6.
[27] Verdaguer-Casadevall A, Hernandez-Fernandez P, Stephens IEL, Chorkendorff I, Dahl S. The effect of ammonia upon the electrocatalysis of hydrogen oxidation and oxygen reduction on polycrystalline platinum. J Power Sources 2012;220:205–10.
[28] Zhao Y, Yu HM, Yang DL, Li J, Shao ZG, Yi BL. High-performance alkaline fuel cells using crosslinked composite anion exchange membrane. J Power Sources 2013;221:247–51.
[29] Paulus UA, Schmidt TJ, Gasteiger HA, Behm RJ. Oxygen reduction on a high-surface area Pt/Vulcan carbon catalyst: a thin-film rotating ring-disk electrode study. J Electroanal Chem 2001;495:134–45.
[30] Yang LJ, Jiang SJ, Zhao Y, Zhu L, Chen S, Wang XZ, et al. Boron-doped carbon nanotubes as metal-free electrocatalysts for the oxygen reduction reaction. Angew Chem Int Edit 2011;50:7132–5.
[31] Wang X, Li MQ, Golding BT, Sadeghi M, Cao YC, Yu EH, et al. A polytetrafluoroethylene-quaternary 1,4-diazabicyclo- 2.2.2 -octane polysulfone composite membrane for alkaline anion exchange membrane fuel cells. Int J Hydrog Energy 2011;36:10022–6.
[32] Zhou J, Guo J, Chu D, Chen R. Impacts of anion-exchange-membranes with various ionic exchange capacities on the performance of H_2/O_2 fuel cells. J Power Sources 2012;219:272–9.
[33] Zeng R, Handsel J, Poynton SD, Roberts AJ, Slade RCT, Herman H, et al. Alkaline ionomer with tuneable water uptakes for electrochemical energy technologies. Energy Environ Sci 2011;4:4925–8.
[34] Unlu M, Zhou JF, Anestis-Richard I, Kim H, Kohl PA. Improved gas diffusion electrodes for hybrid polymer electrolyte fuel cells. Electrochim Acta 2011;56:4439–44.